International Journal of Solids and Structures 46 (2009) 3825–3835

Contents lists available at ScienceDirect

International Journal of Solids and Structures

journal homepage: www.elsevier.com/locate/ijsolstr

Stress–strain behaviour of aluminium alloys at a wide range of strain rates

Y. Chen *, A.H. Clausen, O.S. Hopperstad, M. Langseth

Structural Impact Laboratory (SIMLab), Centre for Research-based Innovation, Department of Structural Engineering, Norwegian University of Science and Technology, NO-7491 Trondheim, Norway

ARTICLE INFO

Article history:
Received 24 July 2008
Received in revised form 1 July 2009
Available online 25 July 2009

Keywords:
Split-Hopkinson bar
Anisotropy
Rate sensitivity
Constitutive modelling
Fracture

ABSTRACT

The stress–strain behaviour of extruded AA6xxx and AA7xxx aluminium alloys in T6 temper was studied at a wide range of strain rates. Tensile tests at low to medium strain rates were performed in a standard tensile test machine, while a split-Hopkinson tension bar was used to carry out tests at high rates of strain. Extruded aluminium alloys have anisotropic mechanical properties, and tests were therefore done in three directions with respect to the extrusion direction. It is found that the AA6xxx alloys exhibit no significant rate sensitivity in the stress–strain behaviour, while moderate rate sensitivity was found for the AA7xxx alloys. There seems to be no significant difference between the rate sensitivity in the three tensile directions. The experimental data were used to identify the parameters of a thermo-viscoplastic constitutive relation for the extruded alloys, which includes the effects of strain hardening, strain-rate hardening, thermal softening and plastic anisotropy.

1. Introduction

Aluminium alloys are attractive for use in automotive parts owing to their low weight. Design and production of light and crashworthy structural parts in aluminium entail development of alloys and manufacturing processes, structural design and crashworthiness analysis. In particular, the increased use of numerical predictions in the design phase calls for material models with a sufficient accuracy and a careful identification of the coefficients involved in the model.

The initial phase of a car crash, involving crushing of the energy absorbing parts of the car body, may be over in fractions of a second. It follows that the rate-of-deformation of these structural components is high. Design of such components based on material properties obtained under quasi-static loading conditions may lead to solutions that are not optimal with respect to dynamic load transfer and energy absorption. In addition, the quest for lighter components leads to stronger utilization of the material and thus to increased probability of fracture. It follows that there is a need for experimental data concerning the dynamic behaviour (i.e. strength and ductility) of aluminium alloys and further for mathematical models of their behaviour that can be used in numerical simulations of crashworthiness.

Tests on aluminium alloys at different strain-rate levels are reported by a number of investigators. Oosterkamp et al. (1999) did compression tests on AA6082 and AA7108 in tempers T6 and T79 at strain rates ranging from 0.1 to approximately 2000 s^{-1}. At room temperature, they found a very low, yet slightly positive, increase in flow stress with strain rate. Similar observations regarding rate sensitivity of aluminium alloys, now in tension, were reported by Reyes et al. (2006), investigating the alloys AA7003-T79 and AA7108-T6. On the other hand, the flow stress and fracture strain of AA6005-T6 were shown by Børvik et al. (2005) to have rather strong positive strain-rate sensitivity. Considering AA7075 in tension as well as compression, El-Magd and Abouridouane (2006) found that the flow stress increases slightly with strain rate, whilst the fracture deformation at increasing rates was reported to increase in compression and decrease in tension. Negative strain-rate sensitivity of flow stress, caused by dynamic strain aging, is found for some alloys in the AA5xxx series, see e.g. Naka and Yoshida (1999), Abbadi et al. (2002) and Clausen et al. (2004). Also measuring the fracture strains in all tension tests at different strain rates, Clausen et al. (2004) found that the fracture strain is rate independent in the dynamic strain aging regime, whilst it increases considerably for higher rates. Smerd et al. (2005) considered the ductility of AA5182 and AA5754 at different strain rates in tension, and reported a small increase in the elongation at fracture.

Tests at a broad range of strain rates are indeed necessary to acquire relevant data for an assessment of crashworthiness behaviour. Keeping in mind that servo-hydraulic test machines rarely can impose a strain rate higher than approximately 1 s^{-1}, other techniques must be applied for obtaining the strain rates occurring in crash situations. A quite recent overview of test methods for elevated strain rates, including drop weights, split-Hopkinson bars and different impact tests, was provided by Field et al. (2004). The split-Hopkinson bar, which may be used in compression, tension and torsion testing, seems to be the most widespread method

* Corresponding author. Tel.: +47 99 73 13 41; fax: +47 37 02 41 28.
E-mail address: yan.chen@bwoffshore.com (Y. Chen).

0020-7683/$ - see front matter © 2009 Elsevier Ltd. All rights reserved.
doi:10.1016/j.ijsolstr.2009.07.013

for material characterization at the crash relevant strain rates because a rather well-defined stress and strain state is feasible (e.g. Harding et al., 1960; Lindholm and Yeakley, 1968; Albertini and Montagnani, 1976; Nicholas, 1981; Staab and Gilat, 1991; Thakur et al., 1996; Verleysen and Degrieck, 2004).

The aim of this paper is to establish data on the stress–strain behaviour of several aluminium alloys with applications in automotive crash components like crash boxes and bumper beams. To this end, tensile tests are performed at a wide range of strain rates using two different testing techniques – a servo-hydraulic testing machine at low and medium strain rates and a split-Hopkinson tension bar (SHTB) at high strain rates. Since the alloys were extruded and exhibit marked anisotropy in strength and plastic flow, tests were performed in three directions with respect to the extrusion direction. In addition to the stress–strain response, the fracture strain was measured on the ruptured specimens. The data obtained from the tests were used to identify the parameters of a thermo-viscoplastic constitutive relation (including strain hardening, strain-rate hardening and thermal softening) and an anisotropic yield criterion for the extruded aluminium alloys.

2. Experimental

2.1. Material

The materials tested were the aluminium alloys AA6060, AA6082, AA7003 and AA7108 in T6 temper. All four alloys were provided by Hydro Aluminium, Sunndalsøra, Norway as extruded rectangular profiles with 10 mm thickness and 83 mm width. The nominal chemical compositions of the materials are shown in Table 1. The materials were solution heat-treated and artificially aged to obtain temper T6 (the peak hardness condition) before machined to test specimens. Alloy AA6060 is recrystallized, while the other alloys have fibrous, non-recrystallized grain structure. Extruded alloys invariably exhibit plastic anisotropy that differs markedly between recrystallized and fibrous grain structures (Li et al., 2005).

2.2. Tension tests

Uniaxial tensile tests at strain rates between 10^{-3} and 10^{3} s^{-1} were performed at room temperature to determine the mechanical behaviour of the extruded aluminium profiles. To investigate the anisotropy of the materials, tensile tests were performed in three directions, 0°, 45° and 90°, with respect to the extrusion direction (ED) of the plate, see Fig. 1. The direction of the test specimens is indicated with an angle α relative to the ED, i.e. $\alpha = 0^\circ$ means that the longitudinal direction of the specimen is parallel with the ED.

The tests were carried out in two different testing devices depending on the strain rate. Uniaxial tests at strain rate between 10^{-3} and 3 s^{-1} were done in a servo-hydraulic test machine, while dynamic tensile tests involving strain rates in the range 100–1000 s^{-1} were performed in a SHTB. For each alloy and direction, 15–17 tests were performed at various strain rates, and the test programme comprised a total of 198 tests. Specification of the test specimen's geometry is provided in Fig. 2. To achieve results unaffected by specimen geometry, the same type of specimen was used in both testing machines. The comparatively small geometrical dimensions were dictated by the SHTB which has a diameter of 10 mm. The initial diameter of each specimen was measured at three different sections in the gauge area of the specimen prior to testing.

Table 1
Nominal chemical compositions of the alloys in wt.%.

Alloy	Fe	Si	Mg	Mn	Cu	Zn	Zr	Al
AA6060	0.19	0.42	0.47	0.015	–	–	–	Bal.
AA6082	0.20	1.04	0.67	0.54	–	–	–	Bal.
AA7003	0.16	0.085	0.62	–	0.038	5.43	0.16	Bal.
AA7108	0.13	0.099	0.87	–	0.031	5.77	0.16	Bal.

For the tests at low to moderate strain rates duplicate tests were carried out for each alloy, direction and strain rate between 10^{-3} and 1 s^{-1}, while only one test was performed for strain rate 3 s^{-1}. This was the highest strain rate which could be obtained without serious noise in the acquired data. The threaded specimen was screwed into purpose-made fixtures and clamped by the hydraulic grips of the machine. A special arrangement was used to avoid any bending moments in the specimen. The tests were carried out in displacement control mode. The strain was measured by a one-sided extensometer with 3.8 mm gauge length. Force, cross-head displacement and strain were logged with a frequency depending on the strain rate. By adjusting the logging frequency, approximately same amount of test data was sampled at all strain rates.

In the SHTB, 6–8 tests at different strain rates between 100 and 1000 s^{-1} were performed for each alloy and direction. As illustrated in Fig. 3, the SHTB consists of two steel bars with a circular cross section and diameter 10 mm: an incident bar AC with length 8140 mm and a transmission bar DE with length 7100 mm. The test specimen is connected by the threaded ends to the bars between C and D. A locking mechanism is located at B on the incident bar, and there is a hydraulic jack at A used to pre-tension part AB. Strain gauges are glued to the bar at the locations 1, 2 and 3. All measurements during the test are based on signals from the strain gauges at 2 and 3, while gauge 1 is used for monitoring the level of the pre-tension force N_0. The bars have a small diameter, and the incoming stress wave, having a length of twice the distance between A and B, is quite long. According to Kolsky (1963), this low diameter to wave-length ratio serves to minimize the dispersion of the stress wave in the set-up shown in Fig. 3. Also, it was checked experimentally with an extra strain gauge glued between lock B and gauge 2 that any dispersion indeed is negligible. Therefore, the strains at point C and D are assumed to be as measured with respectively gauges 2 and 3. The nominal stress s, strain e and strain rate $\dot{e}$ in the sample are then obtained from one-dimensional wave theory (Kolsky, 1963). The sampling frequency was 1 MHz for all tests.

The elastic stiffness determined from the SHTB measurements is in general too low. According to Albertini and Montagnani (1977), the source of this error is the deformation occurring outside the gauge part of the specimen. They suggested to re-calculate the nominal strain as $e = e_0 - s(E - E_0)/(EE_0)$, where e_0 and E_0 are measured values of nominal strain and elastic stiffness, respectively. A standard value of $E = 70,000$ MPa was applied for Young's modulus. Assuming plastic incompressibility, true stress σ and true strain ε were determined from the nominal stress and strain with the well-known relations $\varepsilon = \ln(1+e)$ and $\sigma = s(1+e)$, while the plastic strain was calculated as $\varepsilon^p = \varepsilon - \sigma/E$.

Representative hardening curves in terms of true stress σ and true plastic strain ε^p in three directions at strain rate 10^{-3} s^{-1} are shown in Fig. 4. All curves are drawn to the point of necking. To get rid of noise in the acquired data, the engineering stress–strain curves were smoothed using a moving average with 40 points. It was checked that this smoothing process did not remove important physical information from the test data. The hardening curves in Fig. 4 were then determined based on the smoothed engineering stress–strain curves. It is seen that the fibrous alloys AA6082-T6, AA7003-T6 and AA7108-T6 exhibit marked plastic anisotropy. The trend is that the strength is lower in the 45° direction than in the 0° and 90° directions. The strength is highest in the ED for

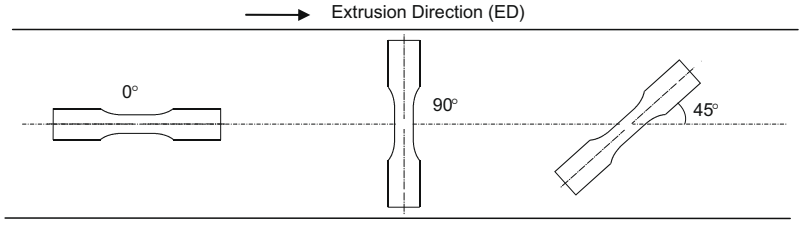

Fig. 1. Orientation of test specimens with respect to the extrusion direction of the flat profile.

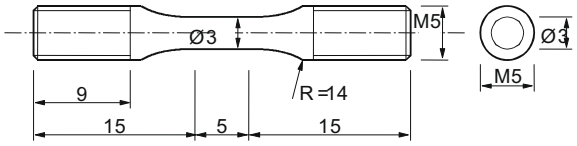

Fig. 2. Geometry of test specimen for tensile tests. Measures in millimetre.

all the fibrous alloys. It is further seen that the plastic anisotropy is stronger for the AA7xxx alloys than for the AA6xxx alloys. For the recrystallized AA6060-T6, the tests at 10^{-3} s^{-1} shown in Fig. 4 indicate some strength anisotropy, where the 90° direction is somewhat stronger than the other two directions. Significant scatter between the duplicate tests was observed for this particular case, and the results are thus somewhat uncertain. However, based on the tests with higher strain rate, it seems that the strength anisotropy of AA6060-T6 is small, which is consistent with previous results for AA6060 in temper T1 (Reyes et al., 2006). For all tests at low to medium strain rate, the average difference between the 0.2% proof strengths obtained from duplicate tests was 3.2 MPa for AA6060, 4.4 MPa for AA6082, 7.6 MPa for AA7003 and 3.7 MPa for AA7108.

In the SHTB tests, the measured stress is only valid for strains beyond some few percent. The reason for this is that the tensile specimen is not in equilibrium in the first phase of the dynamic test. To obtain comparable hardening curves without the small oscillations typically observed in results from SHTB tests, the Voce hardening rule was used to represent each individual true stress-plastic strain curve, i.e.

$$\sigma_f^\alpha = \sigma_0 + Q_R\left(1 - \exp\left(-C_R\varepsilon_\alpha^p\right)\right) \tag{1}$$

where σ_f^α is the flow stress in a tensile test in direction α, ε_α^p is the plastic strain in the same direction, and the strain-hardening parameters σ_0, Q_R and C_R were found by curve fitting. An example of the fitting of the Voce hardening rule in a dynamic test is shown in Fig. 5.

Representative hardening curves for the four alloys in the ED are plotted in Fig. 6 for strain rates between 10^{-3} and 10^3 s^{-1}. The curves are all plotted up to incipient necking. The true stress at 2% and 5% plastic strains vs. true plastic strain rate are plotted for the four alloys in Figs. 7–9, depicting respectively the extrusion, 45° and 90° direction. Data from all tests are presented in these figures, thus, the results from duplicate tests at low to moderate strain rates illustrate the scatter. As one can observe from these figures, alloys AA6060 and AA6082 are rather insensitive to the strain rate, while alloys AA7003 and AA7108 exhibit small, positive strain-rate sensitivity with respect to flow stress. There is no significant difference in the rate sensitivity between the three tensile directions. From Fig. 6 it is further seen that there is some variation in the strain to necking with strain rate for some of the alloys. This indicates that the hardening to some degree depends on the strain rate.

2.3. Plastic anisotropy

To characterize the plastic anisotropy of the alloys, the flow-stress ratio r_α is defined as the ratio between the flow stress σ_f^α in a tensile test in direction α and the flow stress σ_f^0 in a reference test in the ED for the same amount of plastic work

$$r_\alpha = \left.\frac{\sigma_f^\alpha}{\sigma_f^0}\right|_{W^p} \tag{2}$$

where W^p is the specific plastic work. The flow-stress ratio for the reference test in the 0° direction is equal to unity by definition. For a given value of plastic strain ε_α^p, the specific plastic work W^p in a tensile test in the direction α is defined as

$$W^p = \int_0^{\varepsilon_\alpha^p} \sigma_f^\alpha \, d\varepsilon_\alpha^p \tag{3}$$

For each alloy, flow-stress ratios as function of plastic work were calculated up to necking for the 45° and 90° directions. The ratio changes rapidly in the low-strain range of the stress–strain curves, and thereafter it converges to a nearly constant level. A representative value of the flow-stress ratio in the range in which it is approximately constant was computed as specified in Table 2. The values in the table, which were applied in the subsequent calibration of the anisotropic yield criterion, are based on tests at strain rate 10^{-3} s^{-1}.

2.4. Fracture strains

Assuming incompressible plastic deformation and neglecting elastic strains, the fracture strain was obtained from measurements of the original area A_0 and fractured area A_f of the gauge section by $\varepsilon_f = \ln(A_0/A_f)$ (e.g. Dieter, 1988). The fractured surfaces were assumed to have oval shape. The diameters along the long

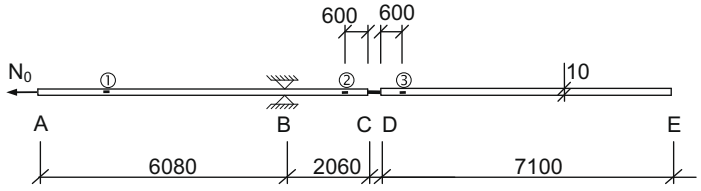

Fig. 3. Schematic overview of split-Hopkinson tension bar. Measures in millimetre.

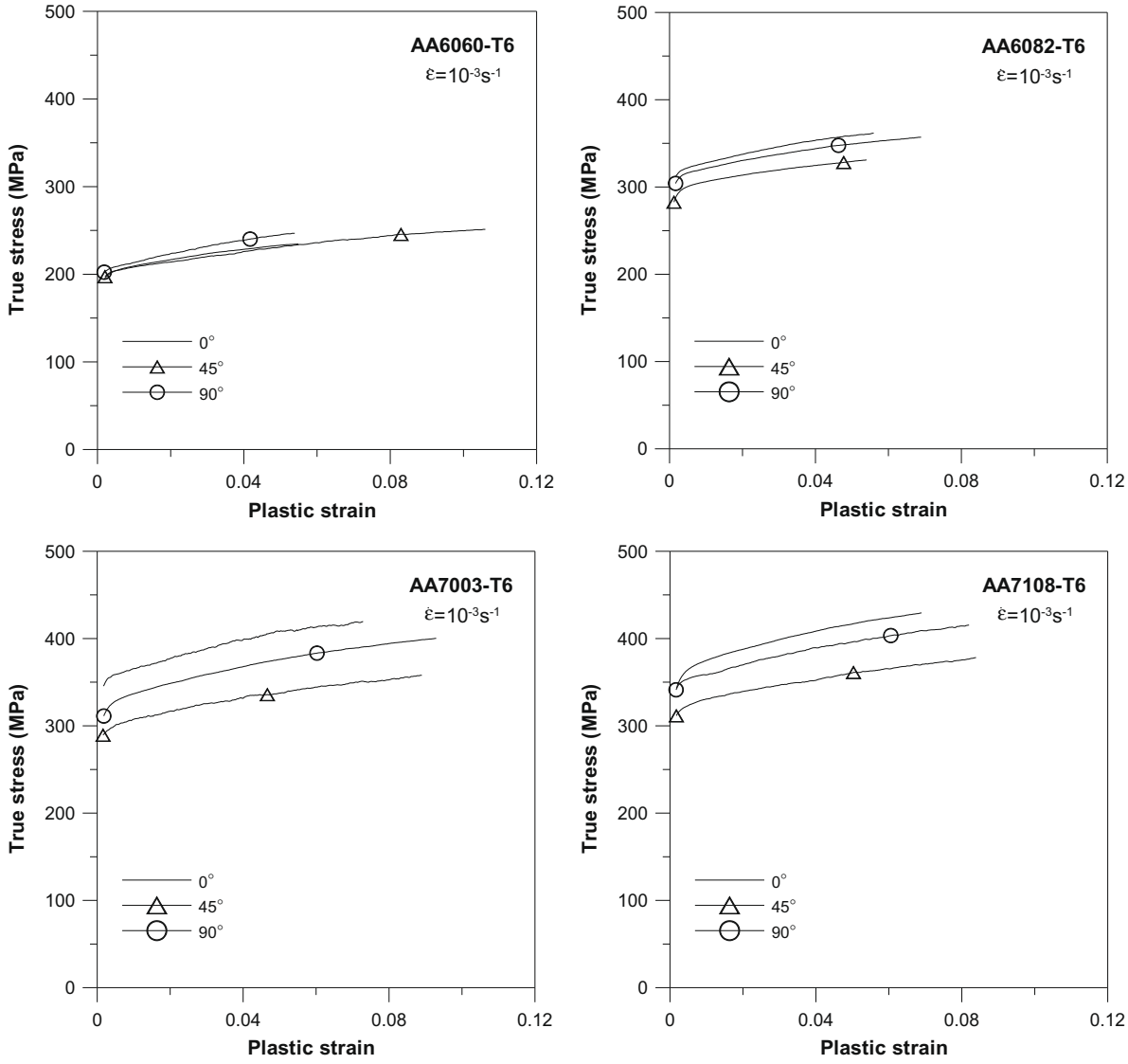

Fig. 4. Representative true stress versus true plastic strain curves showing the plastic anisotropy of the various alloys.

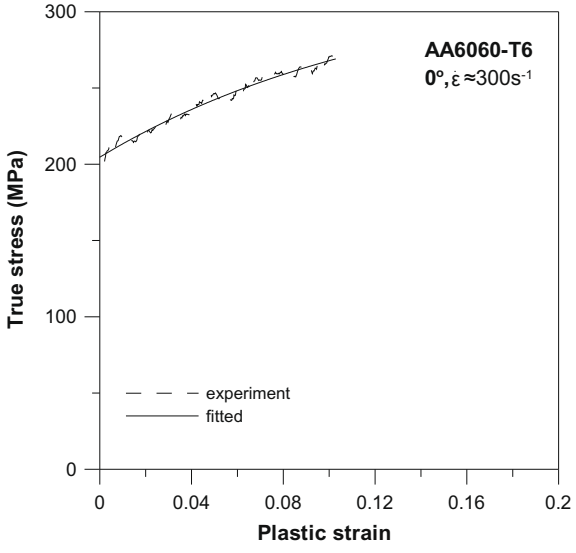

Fig. 5. An example of the fitting of the Voce rule to the measured true stress versus true plastic strain in the dynamic tests.

axis and the short axis of the ellipse were measured with a microscope. Four measurements were made, two for each fractured surface. The fractured area of a specimen was calculated by $A_f = \pi D_1 D_2/4$, where D_1 and D_2 are respectively the average of the measured diameters along the long axis and the short axis of the ellipse for the two fractured surfaces.

The results indicated large scatter in the fracture strain at a given strain rate, and for some alloys and directions a significantly higher fracture strain was obtained for the high-rate tests than for tests at lower rates. The specimens were carefully inspected and it was found that the specimens tested in the servo-hydraulic test machine fell into two categories. In the first, fracture was affected by the small but sharp notch caused by the knives of the extensometer. These specimens most often failed by shear fracture after slight necking or without any sign of necking at all (Fig. 10a). In the second, fracture was not influenced by the extensometer, and the fracture mode was characteristically of cup-cone type with substantial necking (Fig. 10b). This notch sensitivity seemed to be strongest in the ED, and least in the 45° orientation. This is illustrated for alloy AA7003-T6 in Fig. 11. It is seen from the figure that if the specimens that were influenced by the extensometer are disregarded, the influence of strain rate upon the fracture strain

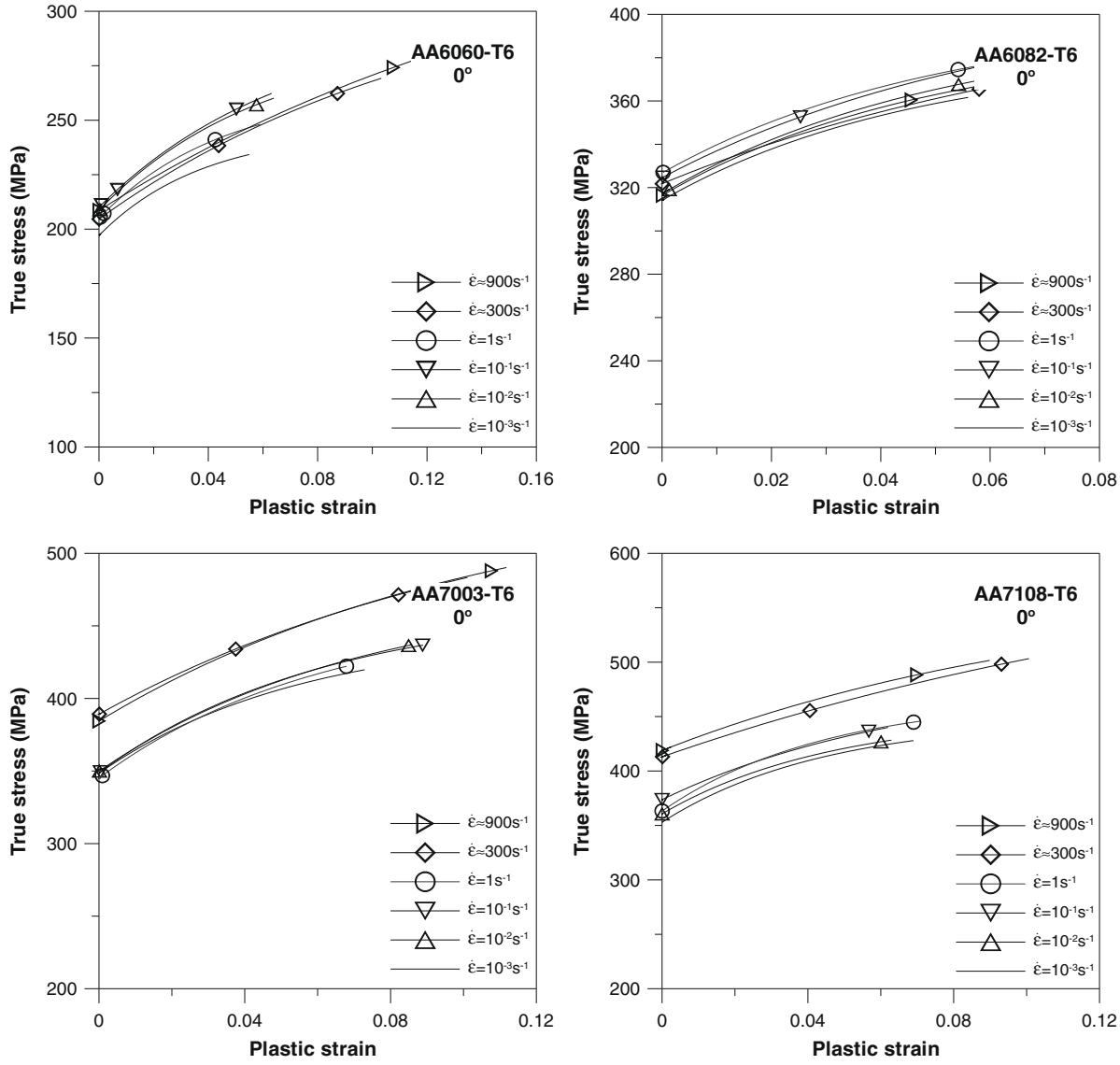

Fig. 6. Representative true stress versus true plastic strain curves showing the strain-rate sensitivity of the various alloys.

seems to be small. This was generally the case. However, the small rate sensitivity could not be established for all combinations of alloy and direction, because in some cases the fracture mode of all specimens at low to moderate strain rates was influenced by the extensometer.

The average fracture strain and its standard deviation from the SHTB tests in the strain rate range 100–1000 s^{-1}, which were all performed without extensometer, are compiled in Table 3. It is seen that the fracture strain is strongly direction dependent. For the recrystallized AA6060 alloy the fracture strain is a great deal lower in the 45° direction than in the two other directions. The trend is opposite for the non-recrystallized alloys, and it is also observed that the fracture strain in the 45° direction is about the same for all four alloys. However, it is clear that AA6060, which is the softest alloy, also has the highest overall ductility in tension. It is finally noted that the measured fracture strains are rather consistent as illustrated by the standard deviations.

The possible scatter was evaluated by performing two test series, each involving 10 samples, on AA6060-T6 in the 45° direction and AA7108-T6 in the 90° direction. These specimens were not equipped with any extensometer, and the tests were carried out at strain rate 0.1 s^{-1}. The average fracture strain was found to be 1.054 and 0.799, respectively, which suggest a slightly higher ductility at this rate than under the dynamic SHTB conditions, see Table 3. The standard deviation in these two test series was respectively 0.076 and 0.023, which is somewhat less than the values reported in Table 3.

3. Constitutive modelling

In this section, the acquired data are used to determine the parameters of a thermo-viscoplastic constitutive model that accounts for strain hardening, rate effects and thermal softening due to adiabatic heating. The model adopts the anisotropic yield criterion Yld91 proposed by Barlat et al. (1991) to describe the plastic anisotropy of the aluminium alloys. We have chosen a relatively simple anisotropic yield criterion since the amount of test data related to plastic anisotropy is rather limited.

3.1. Thermo-viscoplastic constitutive relation

The constitutive relation, which has several similarities with the constitutive relation proposed by Johnson and Cook (1983), reads

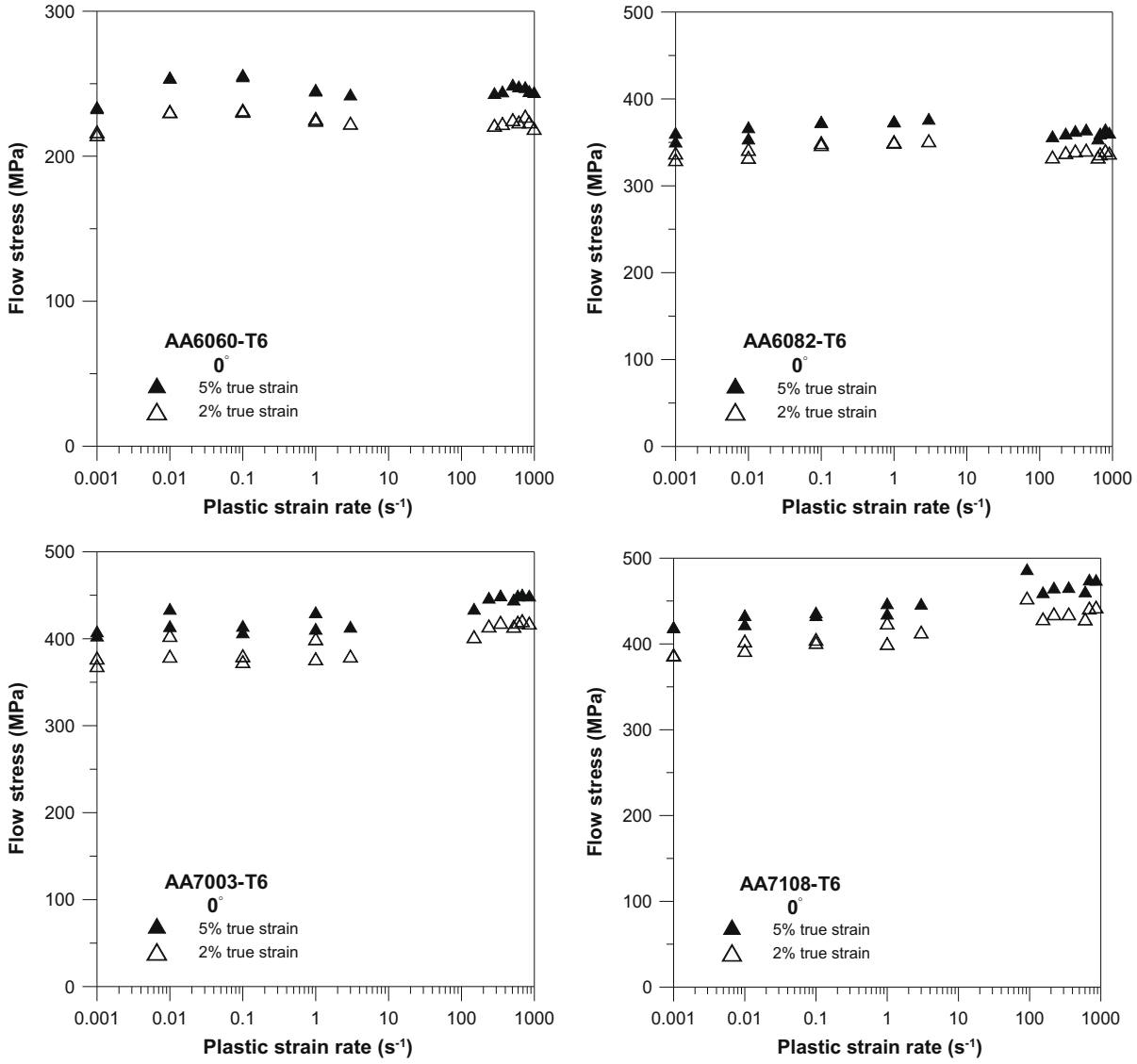

Fig. 7. Flow stress versus plastic strain rate for the various alloys in extrusion direction (ED).

$$\bar{\sigma} = [\sigma_0 + Q_R(1 - \exp(-C_R\bar{\varepsilon}))][1 + \dot{\bar{\varepsilon}}^*]^{C_v}[1 - T^{*M}] \tag{4}$$

where $\bar{\sigma}$ is the effective stress, σ_0 is the yield stress, Q_R and C_R are hardening constants, $\bar{\varepsilon}$ is the effective plastic strain, $\dot{\bar{\varepsilon}}^* = \dot{\bar{\varepsilon}}/\dot{\varepsilon}_0$ is a non-dimensional strain rate, C_v and $\dot{\varepsilon}_0$ are parameters governing the rate sensitivity of the material, M defines thermal softening and T^* is the homologous temperature

$$T^* = \frac{T - T_0}{T_m - T_0} \tag{5}$$

Here, T_0 and T_m are the room temperature and the melting temperature, respectively. Since we are considering loading at high strain rates, it is reasonable to assume adiabatic conditions. In this case, the rate of temperature change is computed as

$$\dot{T} = \chi \frac{\bar{\sigma}\dot{\bar{\varepsilon}}}{\rho C_p} \tag{6}$$

where ρ is the density, C_p is the specific heat capacity at constant pressure, and χ is the Taylor–Quinney empirical constant which specifies the fraction of plastic work converted to heat. A typical value of χ for metals is 0.90.

3.2. Anisotropic yield criterion

The effective stress is defined by the anisotropic yield criterion Yld91 of Barlat et al. (1991), viz.

$$|S_1 - S_2|^m + |S_2 - S_3|^m + |S_3 - S_1|^m = 2\bar{\sigma}^m \tag{7}$$

where S_1, S_2 and S_3 are the principal values of the stress tensor **S**, which in matrix representation reads

$$\mathbf{S} = \begin{bmatrix} \frac{cC-bB}{3} & hH & gG \\ hH & \frac{aA-cC}{3} & fF \\ gG & fF & \frac{bB-aA}{3} \end{bmatrix} \tag{8}$$

In Eq. (8), the variables A, B, C, F, G and H are defined by the components of the Cauchy stress tensor $\boldsymbol{\sigma}$ as

$$A = \sigma_y - \sigma_z, \quad B = \sigma_z - \sigma_x, \quad C = \sigma_x - \sigma_y,$$
$$F = \sigma_{yz}, \quad G = \sigma_{zx}, \quad H = \sigma_{xy} \tag{9}$$

where the x-axis is aligned with the extrusion direction (ED), the y-axis is aligned with the in-plane transverse direction, and the z-axis is aligned with the thickness direction of the profile. The six parameters a, b, c, f, g and h define the plastic anisotropy

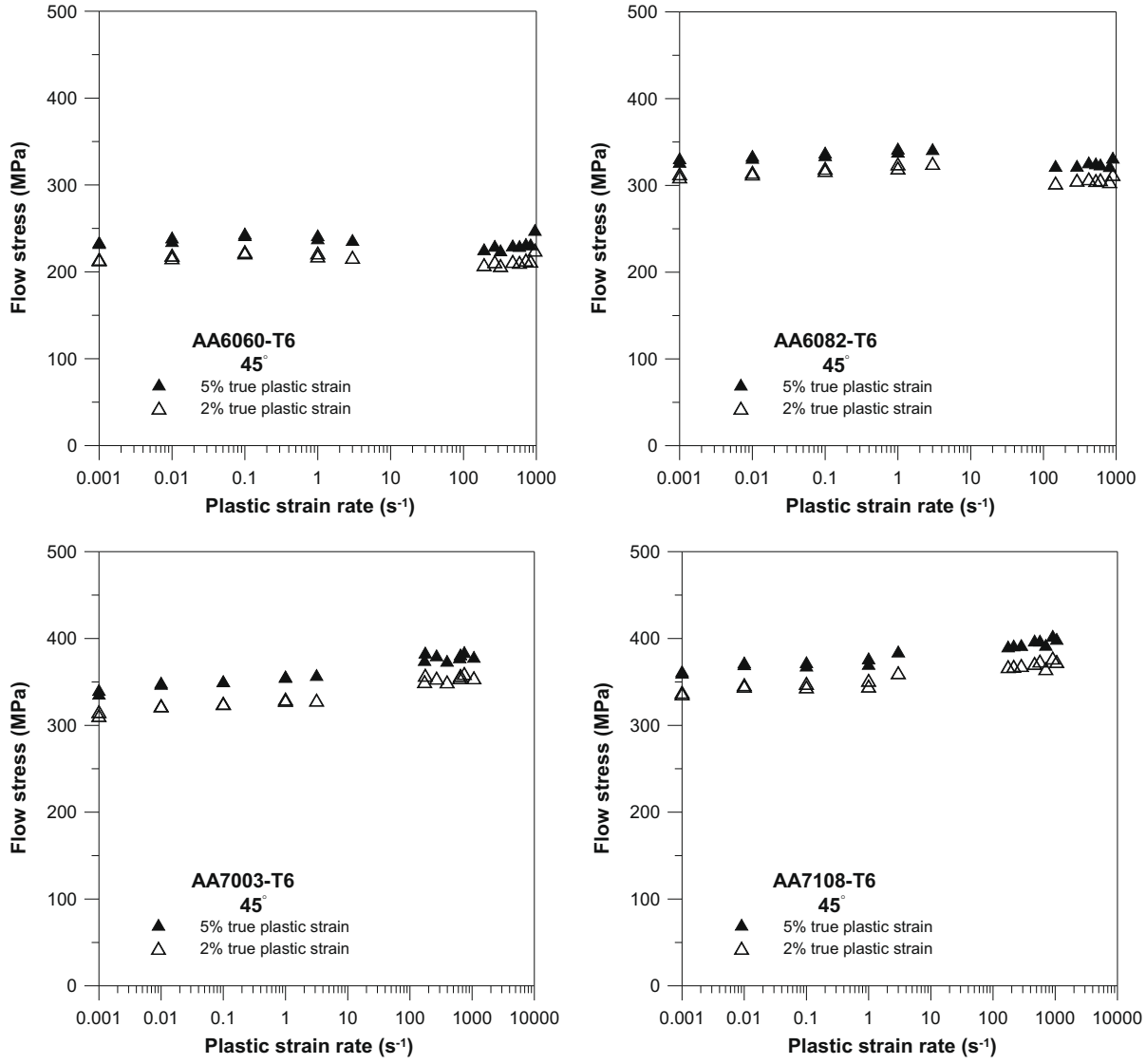

Fig. 8. Flow stress versus plastic strain rate for the various alloys in the 45° direction.

of the material, and are determined from mechanical tests as explained in the next subsection.

3.3. Parameter identification

The constitutive relation, see Eq. (4), consists of three factors governing strain hardening, strain-rate sensitivity and temperature softening. The parameters for each phenomenon were calibrated separately. First, the hardening parameters σ_0, Q_R and C_R were determined from the reference hardening curve in the ED at strain rate 10^{-3} s^{-1}. Although addressing a dynamic test, Fig. 4 clearly shows that the Voce law applied in the first factor of Eq. (4) is able to represent also the stress–strain curves at strain rate 10^{-3} s^{-1} in Fig. 5. With these parameters given, the parameters C_v and $\dot{\varepsilon}_0$ governing the strain-rate sensitivity of the material were determined from flow-stress values at 2% plastic strain for strain rates between 10^{-3} and 10^{3} s^{-1}. Again the data for the ED were used. An example of the resulting strain-rate part of the model, resulting from this identification process, is shown in Fig. 12. Owing to lack of tests at elevated temperature, it was assumed that the flow stress decreases linearly with increasing temperature and thus M was set equal to unity. The resulting material parameters are summarized in Table 4.

The parameters of the anisotropic yield criterion were determined based on the average flow-stress ratios r_α and the R-values, which are defined by

$$R_\alpha = \frac{\dot{\varepsilon}_w^p}{\dot{\varepsilon}_t^p} \tag{10}$$

where $\dot{\varepsilon}_w^p$ and $\dot{\varepsilon}_t^p$ are the plastic strain rates in the width and thickness direction of the tensile specimen. The R-values were not determined in the present experimental investigation. Instead, the R-values for AA6060, AA6082, AA7003 and AA7108 in T6 temper were respectively taken from Jensen (2005), Wang (2006), Achani (2006) and Kokkula (2005), and are summarized in Table 5. Since the R-values of an alloy may vary from one extruded profile to another, the accuracy of these data for the actual rectangular profile is somewhat uncertain.

The yield condition was then calibrated by minimizing the residual

$$\Re = (R_0^{\exp} - R_0^{\mathrm{mod}})^2 + \left(R_{45}^{\exp} - R_{45}^{\mathrm{mod}}\right)^2 + \left(R_{90}^{\exp} - R_{90}^{\mathrm{mod}}\right)^2 \tag{11}$$

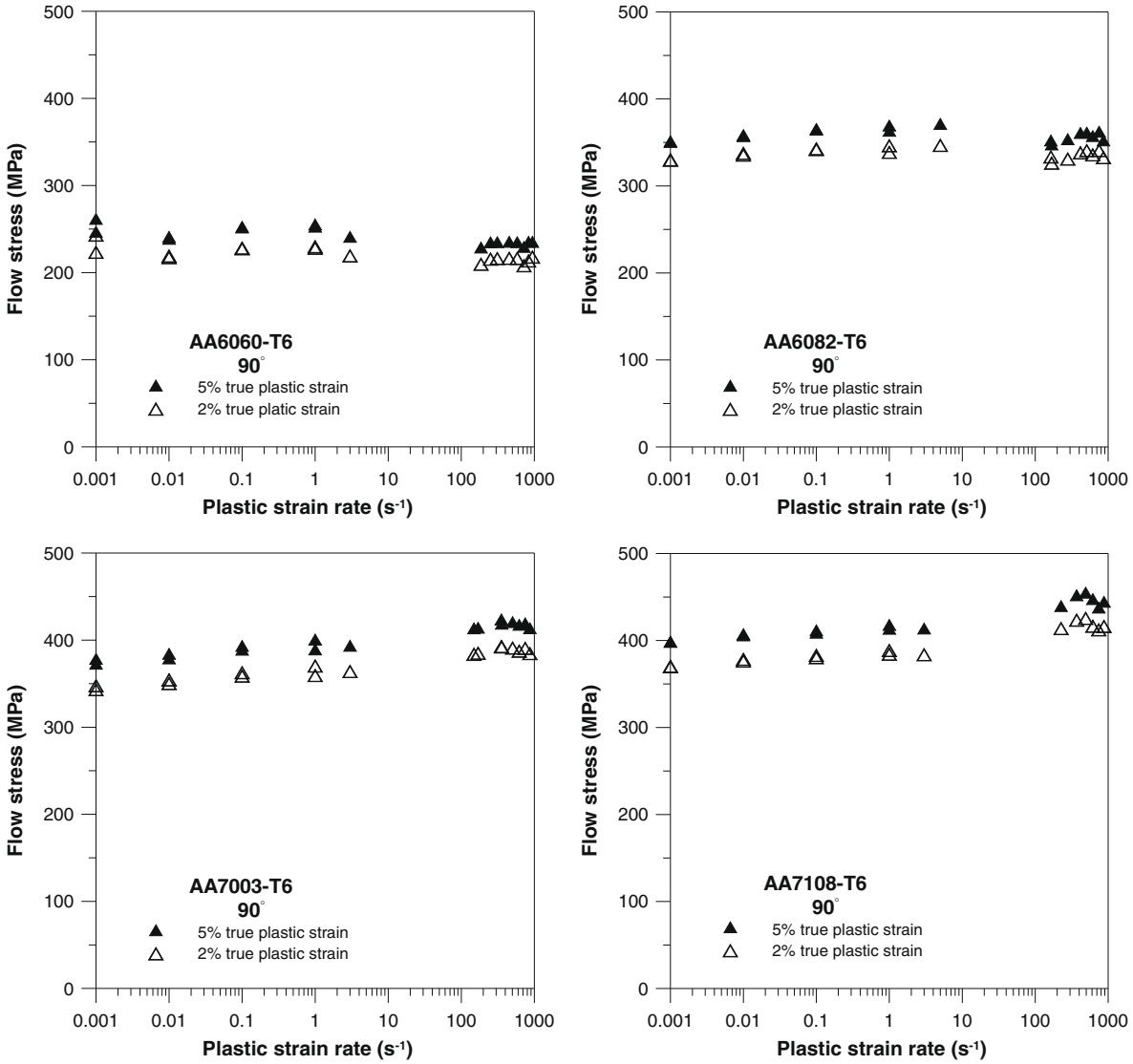

Fig. 9. Flow stress versus plastic strain rate for the various alloys in the 90° direction.

Table 2
Flow-stress ratios for the four alloys at strain rate 10^{-3} s^{-1}.

Alloy	r_0	r_{45}	r_{90}
AA6060-T6	1.0	0.988	1.079
AA6082-T6	1.0	0.919	0.975
AA7003-T6	1.0	0.841	0.923
AA7108-T6	1.0	0.870	0.954

subject to the constraints: $r_\alpha^{\mathrm{mod}} = r_\alpha^{\mathrm{exp}}$ for $\alpha = 0°, 45°, 90°$. The superscripts "exp" and "mod" refer to experimental and model data. The flow-stress ratios r_α^{mod} and R-values R_α^{mod} can be obtained from the constitutive model, using the yield function and the associated flow rule. The exponent m in the yield function is usually given the value 8 for FCC materials such as aluminium (see e.g. Barlat and Lian, 1989). The parameters of the yield criterion are compiled in

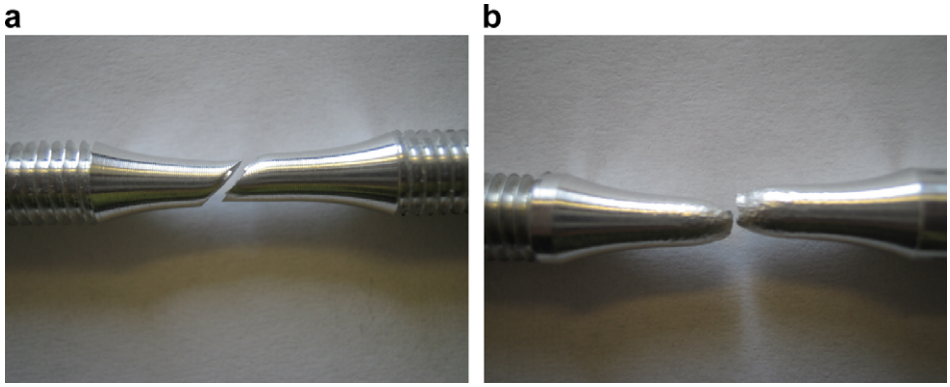

Fig. 10. Fracture modes: (a) shear fracture and (b) cup-cone fracture.

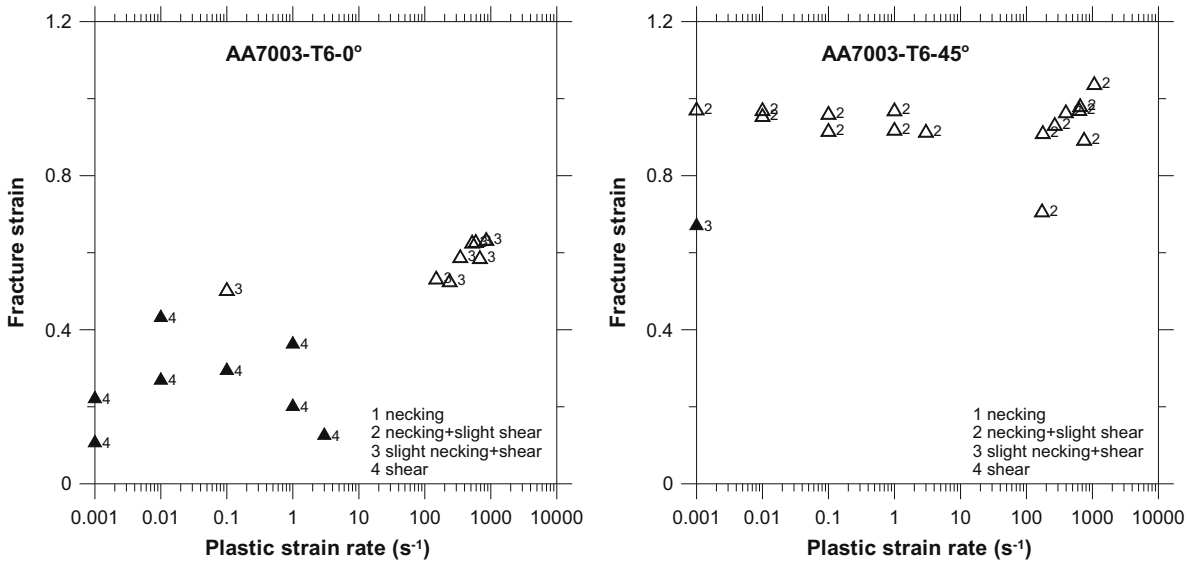

Fig. 11. Fracture strain versus strain rate for alloy AA7003-T6 in the 0° and 45°. The symbols "▲" and "△" indicate fracture influenced by extensometer and fracture not influenced by extensometer, respectively.

Table 3
Average logarithmic strain at fracture from SHTB tests with strain rates between 100 and 1000 s^{-1} for each alloy and tensile direction. The standard deviation is given in parenthesis.

Alloy	Logarithmic strain at fracture, ε_f		
	0°	45°	90°
AA6060-T6	1.530 (0.106)	0.856 (0.095)	1.422 (0.105)
AA6082-T6	0.707 (0.148)	0.901 (0.057)	0.638 (0.127)
AA7003-T6	0.592 (0.045)	0.928 (0.099)	0.785 (0.054)
AA7108-T6	0.579 (0.055)	0.949 (0.077)	0.606 (0.057)

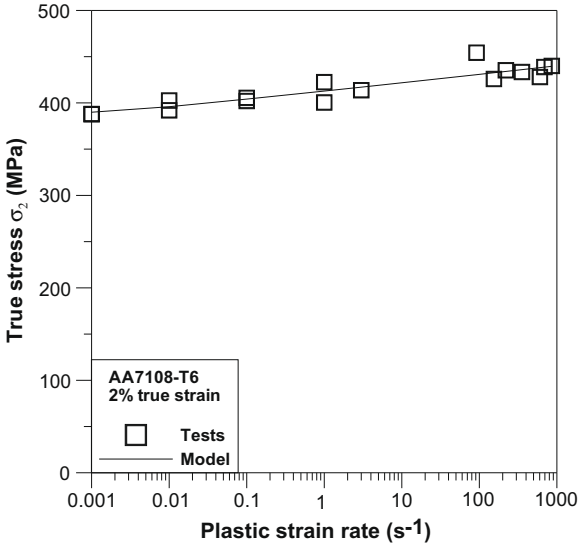

Fig. 12. True stress at 2% plastic strain vs. plastic strain-rate from tests and material model for AA7108-T6.

Table 6. The yield surfaces for AA7003-T6 and AA7108-T6 are depicted in Fig. 13 for a state of plane stress ($\sigma_z = \sigma_{yz} = \sigma_{zx} = 0$). The contours in the figure represent levels of constant normalized shear stress with a contour distance of $0.03\sigma_0$. It is evident that owing to the high exponent and the anisotropy, the shape of the yield

Table 4
Material parameters for the four alloys.

Alloy	σ_0 (MPa)	Q_R (MPa)	C_R	$\dot{\varepsilon}_0$ (s^{-1})	C_v	M
AA6060-T6	196.1	51.2	24.71	0.001	0.0038	1.0
AA6082-T6	310.2	62.7	24.31	0.001	0.0015	1.0
AA7003-T6	344.2	115.7	15.19	0.095	0.0116	1.0
AA7108-T6	354.4	101.1	19.91	0.001	0.0093	1.0

Table 5
Experimental and calculated (in parenthesis) R-values for the four alloys. The experimental values are taken from the literature and are obtained for another set of extruded profiles than those involved in the current study.

Alloy	R-values		
	R_0	R_{45}	R_{90}
AA6060-T6	0.48 (0.51)	0.25 (0.90)	1.38 (0.78)
AA6082-T6	0.37 (0.70)	1.19 (1.09)	0.87 (0.61)
AA7003-T6	0.25 (0.94)	2.11 (1.69)	0.96 (0.58)
AA7108-T6	0.27 (0.43)	0.67 (1.00)	1.16 (0.34)

Table 6
Parameters for YLD91 for the four alloys.

Alloy	m	a	b	c	f	g	h
AA6060-T6	8	0.959	1.098	0.894	1.0	1.0	1.006
AA6082-T6	8	1.098	1.049	0.949	1.0	1.0	1.093
AA7003-T6	8	1.170	1.009	0.991	1.0	1.0	1.218
AA7108-T6	8	1.194	1.106	0.885	1.0	1.0	1.149

surfaces differs significantly from the von Mises ellipsoid. The accuracy of the yield condition can be evaluated by comparing the calculated and experimental R-values. This is done in Table 5 in which the calculated R-values are given in parenthesis. Clearly, the yield function is not able to represent the variation of the R-value with the orientation of the tensile test. However, with the available experimental data it was not found feasible to use an anisotropic yield criterion with more parameters. One possible candidate would be Yld2003-18p (Barlat et al., 2005), but this yield criterion has 18 parameters that need to be determined from a more comprehensive set of experiments or crystal plasticity calculations.

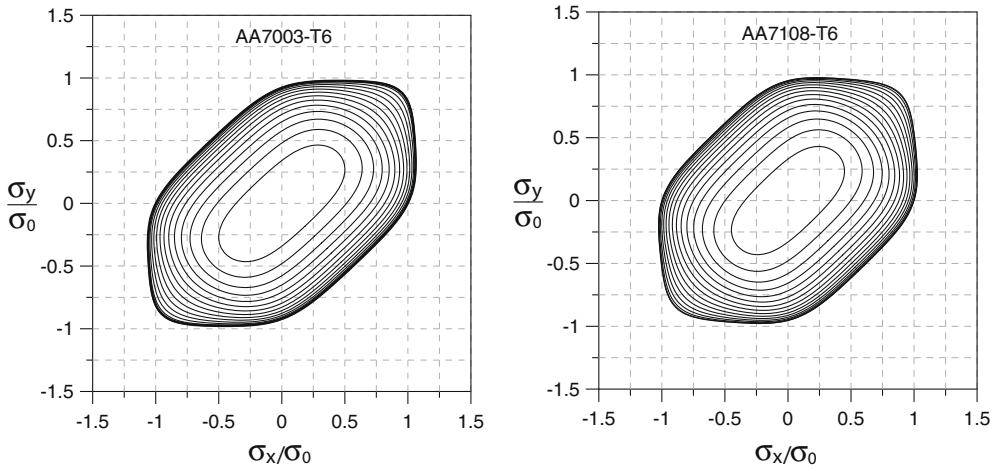

Fig. 13. Yield surface for AA7003-T6 and AA7108-T6 in a state of plane stress ($\sigma_z = \sigma_{yz} = \sigma_{zx} = 0$).

4. Discussion and conclusions

Tensile tests on four aluminium alloys relevant for application in automotive crash components were carried out over a wide range of strain rate, and the stress–strain behaviour and plastic anisotropy were established. Two tests techniques were used to obtain the data. In the low to medium strain-rate range a servo-hydraulic test machine was applied, while a split-Hopkinson tension bar was used for high strain rates.

The tests show that AA6060-T6 and AA6082-T6 exhibit only slight sensitivity to the strain rate, and could probably be modelled as rate-insensitive with good accuracy. AA7003-T6 and AA7108-T6 show a marked sensitivity to strain rate, which should be included in simulations. This is in agreement with earlier observations by Oosterkamp et al. (1999) and Reyes et al. (2006) on similar alloys.

The fibrous, non-recrystallized alloys AA6082-T6, AA7003-T6 and AA7108-T6 have a marked strength anisotropy with the lowest strength in the 45° direction with respect to the extrusion direction. The strength in the 90° direction is somewhat lower than in the extrusion direction. The strength anisotropy for the recrystallized alloy AA6060-T6 is small. The dynamic fracture strain varied with alloy and direction. For the AA6060-T6 alloy the fracture strain was low in the 45° direction and high in the 0° and 90° directions. For the other alloys, the fracture strain was significantly higher in the 45° direction. It is believed that this difference is linked to the different microstructure (texture and grain structure) of the alloys, and is a topic for further investigation in future work.

A possible source of error is the application of two different test devices. The measured data for the alloys presented in Figs. 6–9 indicate, however, that the stress–strain behaviour is consistent in tests performed with the servo-hydraulic machine and the SHTB. Also, earlier investigations reported by Clausen et al. (2004) and Børvik et al. (2005) reveal that the results from the SHTB fit well to the tendency observed from the tests in the servo-hydraulic machine.

A question arising in connection with dynamic material testing is temperature rise. Most of the plastic work in the specimen is converted to heat, and this heat does not have time to be transferred away from the coupon during the duration of a SHTB test. A large temperature increase will of course soften the material and provide hardening behaviour not representative for the assumed room temperature conditions. There was not performed any temperature measurement during the SHTB tests. On the other hand, Eq. (6) can provide an estimate of the temperature increase during the hardening phase up to onset of necking. The nominator in Eq. (6) is the area under the true stress vs. plastic strain curve, which from Fig. 5 is seen to be of order 450 MPa × 0.1. Applying the standard values of $\rho = 2700\ \mathrm{kg/m^3}$ and $C_p = 910\ \mathrm{J/kg\ K}$ for aluminium, the temperature rise is found to be about 15 °C during the part of the test which is relevant for the parameter identification. Earlier investigations suggest that the mechanical properties are only slightly different at room temperature and 100 °C (Clausen et al., 2004; Børvik et al., 2005). Thus, adiabatic heating of the specimen seems to be a minor source of error.

Acknowledgement

The present work was supported by the Research Council of Norway through the strategic university programme "Design of Crashworthy Light Structures".

References

Abbadi, M., Hähner, P., Zeghloul, A., 2002. On the characteristics of Portevin–Le Chatelier bands in aluminum alloy 5182 under stress-controlled and strain-controlled tensile testing. Mechanical Science and Engineering A 337, 194–201.
Achani, D., 2006. Constitutive models of elastoplasticity and fracture for aluminium alloys under strain path change. Ph.D. Thesis, Department of Structural Engineering, Norwegian University of Science and Technology.
Albertini, C., Montagnani, M., 1976. Wave propagation effects in dynamic loading. Nuclear Engineering and Design 37, 115–124.
Albertini, C., Montagnani, M., 1977. Dynamic material properties of several steels for fast breeder reactor safety analysis. Report EUR 5787 EN, Applied Mechanics Division, Joint Research Centre, Ispra, Italy.
Barlat, F., Lian, J., 1989. Plastic behaviour and stretchability of sheet metals. Part I: A yield function for orthotropic sheets under plane stress conditions. International Journal of Plasticity 13, 385–401.
Barlat, F., Lege, D.J., Brem, J.C., 1991. A six-component yield function for anisotropic materials. International Journal of Plasticity 7, 693–712.
Barlat, F., Aretz, H., Yoon, J.W., Karabin, M.E., Brem, J.C., Dick, R.E., 2005. Linear transformation based anisotropic yield functions. International Journal of Plasticity 21, 1009–1039.
Børvik, T., Clausen, A.H., Eriksson, M., Berstad, T., Hopperstad, O.S., Langseth, M., 2005. Experimental and numerical study on the perforation of AA6005-T6 panels. International Journal of Impact Engineering 32, 35–64.
Clausen, A.H., Børvik, T., Hopperstad, O.S., Benallal, A., 2004. Flow and fracture characteristics of aluminium alloy AA5083-H116 as function of strain rate, temperature and triaxiality. Mechanical Science and Engineering A 364, 260–272.
Dieter, G.E., 1988. Mechanical Metallurgy. McGraw-Hill, New York.
El-Magd, E., Abouridouane, M., 2006. Characterization, modelling and simulation of deformation and fracture behaviour of the light-weight wrought alloys under high strain rate loading. International Journal of Impact Engineering 32, 741–758.
Field, J.E., Walley, S.M., Proud, W.G., Goldrein, H.T., Siviour, C.R., 2004. Review of experimental techniques for high rate deformation and shock studies. International Journal of Impact Engineering 30, 725–775.

Harding, J., Wood, E.O., Campbell, J.D., 1960. Tensile testing of materials at impact rates of strain. Journal of Mechanical Engineering and Science 2, 88–96.

Jensen, Ø., 2005. Behaviour of aluminium extrusion subjected to axial loading. Dr.ing Thesis, Department of Structural Engineering, Norwegian University of Science and Technology.

Johnson, G.R., Cook, W.H., 1983. A constitutive model and data for metals subjected to large strains, high strain rates and high temperatures. In: Proceedings of the 7th International Symposium on Ballistics, Hague, pp. 541–547.

Kokkula, S., 2005. Bumper beam-longitudinal system subjected to offset impact loading. Ph.D. Thesis, Department of Structural Engineering, Norwegian University of Science and Technology.

Kolsky, H., 1963. Stress Waves in Solids. Dover, New York.

Li, S., Engler, O., Van Houtte, P., 2005. Plastic anisotropy and texture evolution during tensile testing of extruded aluminium profiles. Model. Simulat. Mater. Sci. Eng. 13, 783–795.

Lindholm, U.S., Yeakley, L.M., 1968. High strain-rate testing: tension and compression. Experimental Mechanics 8, 1–9.

Naka, T., Yoshida, F., 1999. Deep drawability of type 5083 aluminium–magnesium alloy sheet under various conditions of temperature and forming speed. Journal of Materials Processing Technology (89/90), 19–23.

Nicholas, T., 1981. Tensile testing of materials at high rates of strain. Experimental Mechanics 21, 177–185.

Oosterkamp, L.D., Ivankovic, A., Venizelos, G., 1999. High strain rate properties of selected aluminium alloys. Mechanical Science and Engineering A 278, 225–235.

Reyes, Aa., Hopperstad, O.S., Lademo, O.-G., Langseth, M., 2006. Modeling of textured aluminum alloys used in a bumper system: material tests and characterization. Computational Materials Science 37, 246–268.

Smerd, R., Winkler, S., Salisbury, C., Worswick, M., Lloyd, D., Finn, M., 2005. High strain rate tensile testing of automotive aluminum alloy sheet. International Journal of Impact Engineering 32, 541–560.

Staab, G.H., Gilat, A., 1991. A direct-tension split Hopkinson bar for high strain-rate testing. Experimental Mechanics 31, 232–235.

Thakur, A., Nemat-Nasser, S., Vecchio, K.S., 1996. Dynamic Bauschinger effect. Acta Materiala 44, 2797–2807.

Verleysen, P., Degrieck, J., 2004. Experimental investigation of the deformation of Hopkinson bar specimens. International Journal of Impact Engineering 30, 239–253.

Wang, T., 2006. Modelling of welded thin-walled aluminium structures. Ph.D. Thesis, Department of Structural Engineering, Norwegian University of Science and Technology.